Otariidae-Inspired Soft-Robotic Supernumerary Flippers by Fabric Kirigami and Origami

Sicong Liu, Yuming Zhu, Zicong Zhang, Zhonggui Fang, Jiyong Tan, Jing Peng, Chaoyang Song, H. Harry Asada, *Member, IEEE*, and Zheng Wang, *Senior Member, IEEE*

***Abstract*—Wearable robotic devices are receiving rapidly growing attentions for human-centered scenarios from medical, rehabilitation, to industrial applications. Supernumerary robotic limbs have been widely investigated for the augmentation of human limb functions, both as fingers and manipulator arms. Soft robotics offers an alternative approach to conventional motor-driven robot limbs toward safer and lighter systems, while pioneering soft supernumerary limbs are strongly limited in payload and dexterity by the soft robotic design approach, as well as the fabrication techniques. In this article, we proposed a wearable supernumerary soft robot for the human forearm, inspired by the fore flippers of otariids (eared seals). A flat flipper design was adopted, differing from the finger- or arm-shaped state-of-the-art works, with multiple soft actuators embedded as different joints for manipulation dexterity. The soft actuators were designed following origami (paper folding) patterns, reinforced by kirigami (paper cutting) fabrics. With this new approach, the proposed soft flipper incorporated eight independent muscles, achieving over 20 times payload to self-weight ratio, while weighing less than 500 g. The versatility, dexterity, and payload capability were experimentally demonstrated using a fabricated prototype with proprietary actuation and control. This article demonstrates the feasibility and unique advantages of origami + kirigami soft robots as a new approach to strong, dexterous, and yet safe and lightweight wearable robotic devices.**

***Index Terms*—Actuators, pneumatic systems, robots, soft robotics.**

Manuscript received May 11, 2020; revised September 7, 2020; accepted December 9, 2020. Date of publication December 17, 2020; date of current version October 14, 2021. Recommended by Technical Editor J. Park and Senior Editor G. Alici. This work was supported in part by NSFC under Grant 51975268, in part by Hong Kong ITF under Grant ITS/140/18, in part by SUSTECH-AISONO Joint Lab Grant, and in part by SUSTech-MIT Joint Centers for Mechanical Engineering Education and Research. *(Corresponding author: Zheng Wang.)*

Sicong Liu and Chaoyang Song are with the Department of Mechanical and Energy Engineering, Southern University of Science and Technology, Shenzhen 518055, China, and also with the Guangdong Provincial Key Laboratory of Human-Augmentation and Rehabilitation Robotics in Universities, Department of Mechanical and Energy Engineering, Southern University of Science and Technology, Shenzhen 518055, China (e-mail: liusc@sustech.edu.cn; songcy@ieee.org).

Yuming Zhu and Zicong Zhang are with the Department of Mechanical and Energy Engineering, Southern University of Science and Technology, Shenzhen 518055, China (e-mail: 11711107@mail.sustech.edu.cn; 11711203@mail.sustech.edu.cn).

Zhonggui Fang and Jiyong Tan are with the Department of Mechanical and Energy Engineering, Southern University of Science and Technology, Shenzhen 518055, China, and also with the SUSTECH-AISONO Joint Laboratory of Medical Robotics Research, Southern University of Science and Technology, Shenzhen 518055, China (e-mail: 11930523@mail.sustech.edu.cn; scutjy2015@163.com).

Jing Peng is with the Department of Mechanical Engineering, University of Hong, Hong Kong SAR, China (e-mail: jingyyhnzg@gmail.com).

H. Harry Asada is with the Department of Mechanical Engineering, Massachusetts Institute of Technology, Cambridge, MA 02139 USA (e-mail: asada@mit.edu).

Zheng Wang is with the Department of Mechanical and Energy Engineering, Southern University of Science and Technology, Shenzhen 518055, China, with the SUSTECH-AISONO Joint Laboratory of Medical Robotics Research, Southern University of Science and Technology, Shenzhen 518055, China, with the Guangdong Provincial Key Laboratory of Human-Augmentation and Rehabilitation Robotics in Universities, Department of Mechanical and Energy Engineering, Southern University of Science and Technology, Shenzhen 518055, China, and also with the Department of Mechanical Engineering, University of Hong Kong, Hong Kong SAR, China (e-mail: zheng.wang@ieee.org).

This article has supplementary material provided by the authors and color versions of one or more figures available at https://doi.org/10.1109/TMECH.2020.3045476.

Digital Object Identifier 10.1109/TMECH.2020.3045476

I. Introduction

SUPERNUMERARY robotic (SR) devices augment extra limbs worn by the human user to enhance their manipulation capability [1], [2], [4], [8], [9], [11]. Various existing works on SR devices have thoroughly demonstrated the feasibility for such devices [7], [11], [12], as well as their efficacy in restoring grasping functions resulting from hand motoring deficiencies due to trauma, stroke, and neurological injuries [1]. Reported works in literature augmented one [6], [7], [10], [12], [13] or multiple [1], [2], [29] extra fingers to the human wearer's forearm for supernumerary grasping, with two fingers the vast majority [3], [4], [5], [15], [16]. Driven by in-situ electric motors [6], [12], [32], off-board motors with cable-conduit transmission [9], or soft actuators [7], [15], [17], the contact forces and self-weight for existing systems could vary across a wide range from 5.7 to 8.2 N, and from 200 to 750 g [3], [6], [7], [18], respectively, but mostly sufficient for activities of daily living (ADL) [10], [14]. However, their mechanisms, rigid, or soft, added significant weight and bulkiness to the wearer, severely hindering the forearm's wearing comfort and reachability, while constantly presenting notable visual cues. A soft, low-profile, dexterous, and lightweight approach is therefore desirable, to provide stealth but task-effective alternative.

Nature provides us with abundant inspirations for robot design. Otariidae family animals (eared seals) have the most prominent forelimbs (flippers) in the Pinniped clade (see Fig. 1), both for underwater propulsion, predating, and object holding [20], [21], [22]. The pair of large, strong, and dexterous fore flippers

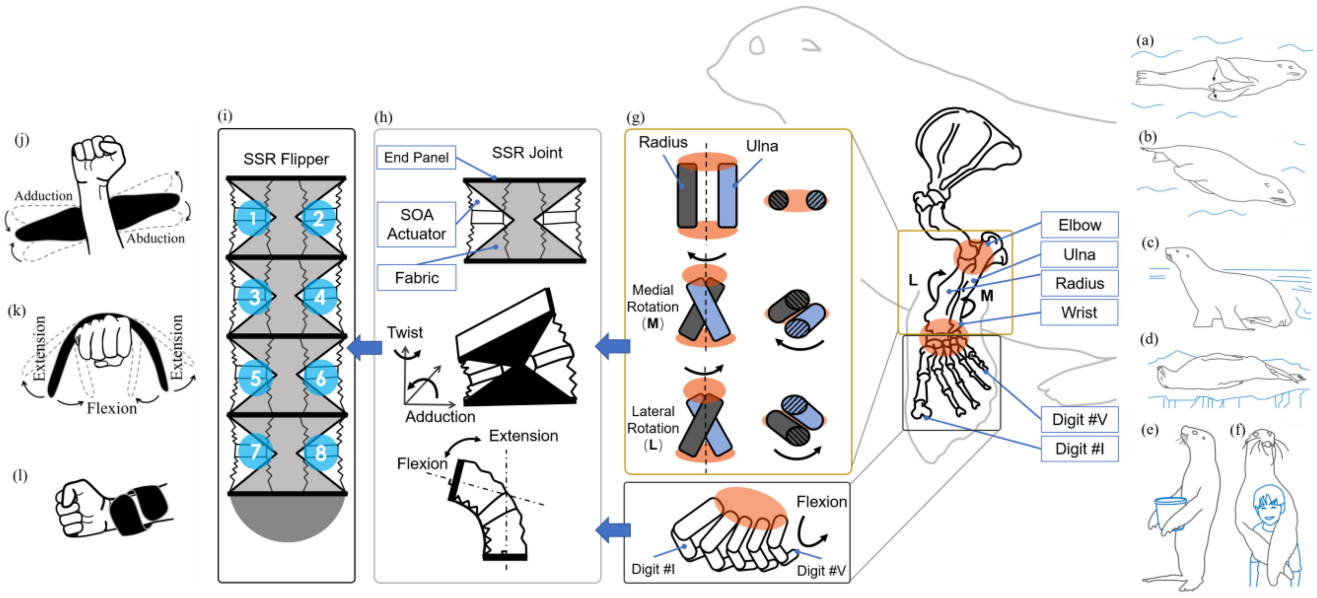

Fig. 1. Inspiration from Otariidae fore flippers for the proposed SSR flippers. The flat profile and dexterity of the fore flippers of Otariidae maximize the propulsion efficiency in (a) propulsive phase of the aquatic locomotor cycle, and in (b) recovery phase, the flippers can be folded to the torso to keep streamline; the flippers move accordingly when Otariidae carries out unique activities, such as (c) terrestrial walking, (d) resting, (e) object handling, and (f) hugging. (g) Radius and ulna of the forearm twist during medial and lateral rotation of the flipper, while keeping a flat cross-sectional shape; the flipper phalanges enable smooth bending of the distal flipper end for swimming and object handling. Taking inspirations of the forearm and digits, (h) two actuators are fixed parallelly to form an SSR joint with a flat profile, when one actuator inflated and the other deflated, the joint outputs abduction or adduction; a piece of non-stretchable fabric constraint is attached to the joint, such that when both actuators inflated simultaneously, the joint outputs flexion and extension. The fabric constraint is non-stretchable in both in-plane directions but flexible in other directions. (i) Four SSR joints are stacked sequentially to form an SSR flipper with both eight-DOF dexterous motion and a flat surface. The proposed SSR flippers are designed to be worn on the human forearm, the abduction and abduction movements are defined in (j); (k) definition of flexion and extension movements; and (l) SSR flippers can compactly yet comfortably wrap around human forearm.

of otariids is capable of both swimming underwater and terrestrial walking, as well as performing various highly dexterous object-handling circus tricks after training [19], [23], [24]. However, during swimming or gliding on land, their fore flippers could be folded beside their torso without hindering streamlining [20]. This unique combination of strength, dexterity, and foldability for the Otariidae flippers provides an ideal source of inspiration for the design of robotic supernumerary limbs in this article.

In this article, a supernumerary soft robotic (SSR) flipper is proposed, inspired by Otariidae fore flippers [see Fig. 1(g)], toward a soft, lightweight, low-profile, and dexterous alternative to existing solutions. Different from state-of-the-art SR limb designs, the proposed SSR flipper comprises entirely of soft components, with kirigami fabric constraints over origami soft actuators, achieving superior dexterity, strength, light weight, and foldability. The main contributions are summarized as follows:

1) Proposed an Otariidae-inspired flat SSR joint design, achieving two degrees-of-freedom (DOF) bending (flexion and extension) + deflection (adduction and abduction) deformation using two parallel soft muscles, and the joint design is stackable with multiple sequential segments composing the entire flipper.
2) Proposed an origami + kirigami approach in fabricating the SSR joints, with kirigami fabric constraints acting over soft origami actuators (SOAs) to predefine the joint motions. This resulted in the entire structure being soft and flexible, while the inextensibility of fabrics ensured sufficient payload capability for ADL.
3) Proposed an Otariidae-inspired SSR flippers system design with one pair of foldable flippers of eight DOFs. Design validation by experimental evaluation with an SSR flippers prototype driven by pneumatic actuation.

The rest of this article is organized as follows. The conceptual design of the SSR flippers is presented in Section II. Section III presents the origami and kirigami approach to the SSR joint, followed by flipper design and implementation in Section IV. Experimental validations of the actuator, joint, and the flippers are presented in Section V, and finally, Section VI concludes this article.

II. Concept of Otariidae-Inspired SSR Flippers

SR devices are used to enhance the human user's manipulation capability, which should have the following three desired features.

1) Low profile: The device could be foldable tightly to the human forearm when not being used, presenting minimum interferences to normal user activities.
2) Lightweight: The entire wearable piece should present low self-weight for the user to bear.
3) Functional: The SSR should have both the dexterity and payload to suit ADL.

To achieve the above unique feature list, unconventional approaches are needed. The fore flippers of Otariidae are flat in

shape compared to the columnar human fingers or limbs. Compared with other flat shape limbs, such as bird wings, the flippers of Otariidae possess an advantage in dexterity which enables the sea lions to accomplish tasks other flat-limb animals cannot. Its flat profile and dexterity maximize the propulsion efficiency underwater in the propulsive phase of the aquatic locomotor cycle [see Fig. 1(a)]. While in the recovery phase [see Fig. 1(b)], the flippers are closely folded to the torso to obtain streamline and thus reduce drag [19]. Thanks to the dexterity of the fore flippers, the Otariidae are able to perform agile and sophisticated activities such as underwater maneuvers, terrestrial walking and object handling, and hugging [see Fig. 1(c)–(f)].

SR devices require high dexterity and compactness for daily use. The flat-shaped flippers of Otariidae provide valuable inspiration to the SSR flipper. Apart from the flat shape and dexterity of the flipper, the detailed anatomic structure of the Otariidae flipper also provides design cues. The skeletal model of the fore flipper and the principle of inspiration is shown in Fig. 1(g). The forearm section consists of two parallel bones (Radius and Ulna), enabling twisting of the joint (Medial and Lateral Rotation) while keeping a flat cross-sectional shape; while the flipper phalanges enable smooth bending of the distal flipper end for swimming and object handling. Taking inspirations from the forearm and digits, we proposed an integrated SSR joint with two DOFs [see Fig. 1(h)], combining bending and twisting within one joint.

The distal flipper end where the digits reside is covered with membranes to create a flat and smooth surface, both for swimming and object handling. Inspired by this, we introduced a kirigami constraining layer over the origami muscles, both as flat-shaped motion constraints and an interfacing layer for object handling. Therefore, we could achieve an SSR design with both eight-DOF dexterous motion and a flat surface. However, here we stacked the forearm-and-digit-inspired SSR joint across the flipper to increase motion range. This is not strictly following the kinematic structure of the Otariidae flippers.

Each SSR joint includes two parallel SOAs [see Fig. 1(h)].With appropriate constraints, the motion of two actuators is coupled to generate flexion and abduction in perpendicular planes. The SSR joint generates flexion or extension when both actuators extending or contracting simultaneously. It performs abduction and adduction when actuators deform antagonistically.

For maximum safety and wearing comfort, the SSR flipper was designed to be entirely soft, with the structure constructed only using soft materials, such as fabrics and elastomers. Thus, the SSR flippers can be wrapped around the user's forearm similarly to the foldable flippers on otariids. Compared with the conventional rigid robotic supernumerary fingers with servo motors and linkages, the SSR flipper is more compliant and evenly distributed in a flat profile [1], [3]. They are even more compliant than existing soft SR fingers [1], [7], [15], by avoiding all rigid components.

In this paper, an origami + kirigami approach was proposed to design soft robots with high payloads and yet fully-soft body structures. High efficiency origami-patterned soft actuators were used to generate large motion range and high forces at moderate air pressures, while kirigami fabrics were used to reinforce the soft actuators to direct the loading forces to their non-stretchable directions, while the entire assembly remaining soft on the other, flexible directions of the reinforcing fabrics.

A new "hugging" pattern of object interaction was introduced, following the flat-shape flippers for the proposed SSR design, in addition to grasping and pinching. Moreover, with the constrain effect of the non-stretchable fabric, the hugging pattern can significantly increase the load capacity. To fully utilize this advantage, the proposed pair of SSR flippers are to be worn on the wrist of the user with its shoulder located at the back side of the human forearm [see Fig. 1(j)–(l)], maximizing the contacting area between the SSR flippers and forearm, improving interaction reliability.

Finally, to achieve a lower profile for the wearer, the SSR flippers can wrap around the forearm without overlapping [see Fig. 1(l)], significantly reducing the overall diameter of the device when being worn, causing less obstructions in daily use.

III. Origami + Kirigami Approach to SSR Joint

In order to achieve a flat shape, light-weight, wearing comfort, and dexterity, an SSR joint consists of two SOAs, and a Kirigami fabric strip was proposed with two-DOF movements.

A. Origami Soft Actuator

Powerful, efficient, and programmable movements of SOAs have been achieved in existing works 28], [30], [31], where origami mechanisms were used as motion constraints to either preprogram [30] or reinforce soft robotic actuators [31]. These actuators assemble at least two components to obtain desired actuation functions [28], [30], [31]. The complexity in fabrication hinders the repeatability of actuator's performance, especially, in mass production.

To achieve mass-production-ready one-step fabrication of the actuator, the highly commercialized compliant material and cost-efficient industrial fabrication process were chosen, which are Ethylene-Vinyl Acetate Copolymer (EVA) by FORMOSA and blow molding, respectively, as shown in Fig. 2. The proposed SOA consists of one air-tight internal chamber directly constructed by the origami mechanism as in [25]. This pattern is also a variation of the well-known Yoshimura pattern, which consists of trapezoid facets other than triangles.

The origamic mechanism substantially reduces material stretch, compared to stretch-based actuation generation in silicone-rubber soft actuators and, therefore, improves actuation efficiency. The repetitive trapezoid facets and prismatic layers lead to simple customization for a desired mechanical property. A stable linear axial movement is induced by origami-like folding and unfolding when pressurized within the chamber.

To obtain the optimal design of the origami pattern, variations of Yoshimura origami patterned tubes were modeled and tested in the finite element method simulation as shown in Fig. 2(g)–(k). The simulations were carried out in Abaqus/Standard. The material of the tubes was set as elastic with Young's Modulus 30 MPa and Poisson's ratio 0.3. The element type of the FE model is Tet. The geometric parameters of the origami patterns are defined and listed in Tables I and II.

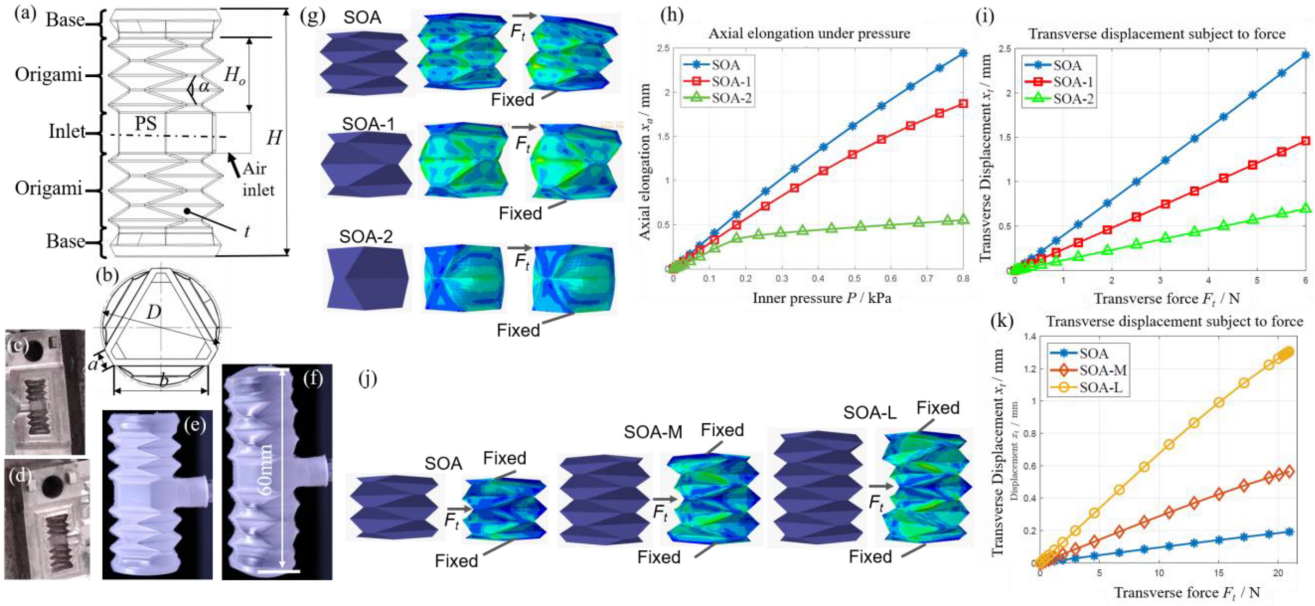

Fig. 2. Design, simulation, and fabrication of SOA. (a) Parameters of the SOA are defined, (b) cross section of the SOA. The SOA is made by blow molding; (c) female and (d) male molds for the blow-molding process are shown. (e) SOA is made of EVA material. (f) Maximum elongation reaches 60 mm when pressurized. (g) Simulations were carried out on the origami pattern, SOA, SOA-1, and SOA-2. (h) SOA pattern extends significantly longer than the other two when applied the same inner pressure, (i) SOA pattern deforms the largest when subjected to transverse force in the radial direction. (j) Simulation result shows the longer actuator is more likely to deform when subject to transverse force.

TABLE I
GEOMETRY OF THE SOA

H	Height of SOA	42mm
H_o	Height of the origami section	13mm
t	Thickness of origami facet	0.5mm
α	Dihedral angle of two trapezoid facets	65.6°
D	Diameter of the circumcircle	20mm
a	Length of short parallel side of facet	2.9mm
b	Length of long parallel side of facet	15.1mm
H_{max}	Length of SOA when fully pressurized	60mm
H_{min}	Length of SOA when fully depressurized	20mm

TABLE II
GEOMETRY OF THE ORIGAMI PATTERNS

Design	H mm	α	N	H mm	r_a mm	r_b mm
SOA	5	65.68°	2.5	12.5	5.99	10
SOA-1	8.33	94.18°	1.5	12.6	5.91	10
SOA-2	25	145.57°	0.5	12.7	5.91	10
SOA-M	5	65.68°	3.5	17.5	5.91	10
SOA-L	5	65.69°	4.5	22.5	5.91	10
Bellow	5	65.68°	6	42	5.91	10

As shown in Fig. 2(g), the SOA, SOA-1, and SOA-2 are similar in height and diameter but different in the density of origami pattern. At the same height, SOA has the highest number of origami layers, which displayed a larger axial elongation in Fig. 2(h). The SOA showed the largest transverse deformation when subjected to radial loading [see Fig. 2(i)].

The SOA, SOA-M, and SOA-L consist of the same origami pattern while different in axial height. As shown in Fig. 2(j) and (k), the shortest SOA is considerably more stable under transverse loading. As a result, the SOA design was chosen to construct the origami actuator in consideration of both ranges of motion and stability.

To achieve an easy assembly of the actuator to the supporting structure, the air inlet was located in the middle of the SOA. Two base sections at both ends are intended for easy mounting. The actuator outputs one DOF linear translation along its axis. The deformation of two origami sections is symmetric to the plane of symmetry [see Fig. 2(a)] when pressurized inside. The principal geometry parameters are shown in Table I. The weight of each SOA is 1.8 g. The SOA extends to a total length of 60 mm when fully pressurized, contracts to 20 mm when fully depressurized, with a 40 mm stroke.

An analytical model of the actuator has been derived in [26]. The relationship is given as follows:

$$F = F_k(\beta) + F_p(P_m) \tag{1}$$

where $F_p(P_m)$ is the force induced by the relative pressure in the chamber P_m. $F_k(\beta)$ is the force generated by spring-like deformation β. F_p can be obtained as

$$F_p = SP_m \tag{2}$$

where S is the effective area of the actuator. The force F_k is obtained as follows:

$$F_k = k\beta \tag{3}$$

where k is the equivalent coefficient of elasticity of the SOA.

B. Kirigami Fabric Constraints

Soft rotary actuators intended for robotic joints have been studied showing promising perspectives. The rotary elastic chamber actuator applies elastic bellows into a concise, rigid rotary joint to output rotary movement with natural compliance [29]. The soft origamic rotary actuators utilizing 3D-printed origami chamber to construct a rotary joint with enhanced strength, servo performance, and impact behavior shaping [27]. However, the movements of such actuators are limited to rotation, hence the bulky volume makes them inapplicable in our case.

The use of patterned fabrics, origami structures, and kirigami techniques to constrain soft robot's motions and/or toward force enhancements have been reported by literature. The main approaches could be summarized by the following:

1) Using patterned surfaces (paper, polymer, or fabrics) around a soft robotic actuator (constrained or unconstrained) to achieve interfacing and surface features, such as the crawling soft bot presented in [33] and the kirigami-enhanced soft actuator in [34].
2) Using fabrics to wrap a soft robotic actuator to achieve motion definition or force enhancement, such as the wearable fabric actuators in [35]. To generate angular elongation from the origami extension actuators, an approach utilizes the paper–elastomer strip to partially constrain the local expansion of the pleats was proposed in [28].
3) Origami soft robots where the folded origami structures served as motion constraints themselves, as surveyed by [36].

Different from the existing works, in this article, we deliberately separated individual actuator motion constraints (by origami) from the over-all SSR flipper motion constraints (by kirigami). By doing this, we could use a single design of SOAs, mass-produced using industrial fabrication techniques, and compose various, dexterous SSR robotic devices by changing the kirigami patterns.

The bellow actuators are similar to the proposed origami actuator in terms of the range of motion and mass-production capability. FE simulations were carried out in Abaqus to differentiate the characteristics of the bellow and SOA actuators. The geometric parameters of both actuators are listed in Tables I and II. The simulation results are presented in Fig. 3(a)–(d). The bellow actuator outputs larger elongation when pressurized than the SOA actuator, while the SOA actuator deforms less than the bellow actuator when subjected to radial force. Thus, in constructing the SSR flippers, the SOA actuators were chosen to enhance the stability of the system.

In this article, intended for the wearable SSR flippers, the non-stretchable Nylon fabric strip is utilized to constrain the linear axial movement of the SOA. By applying EVA adhesives (from glue gun) on the bonding areas between the fabric and actuator [see Fig. 3(e)], the local elongation of SOA was limited. Thus, the linear movement of the actuator is constrained by the fabric, the resultant angular-elongation is obtained. When pressurized, two end faces of the actuator rotate relatively. It is noteworthy that the side facets of the SOA, including the Base, Inlet, and

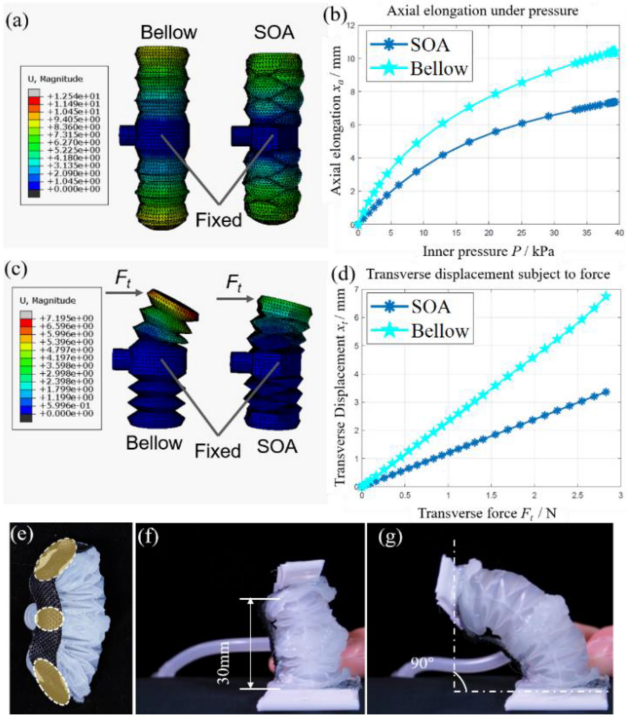

Fig. 3. Comparison between the origami patterned actuator and the conventional bellow actuator were carried out in simulation. (a) When pressurized simultaneously, the bellow actuator outputs larger axial elongation than the SOA actuator; the pressure and elongation relationship is shown in (b). (c) When subjected to transverse force in the radial direction, the SOA actuator showed superior stability, i.e., smaller deformation caused by the transverse force than the bellow actuator (d). (e) Nylon strip was glued to the end faces and side of SOA with EVA adhesive, the glued areas are marked; the constrained SOA (f) contracted to its minimum length when depressurized and (g) angular elongation up to 90° when pressurized.

Origami sections, should be fixed to the Nylon strip to avoid buckling of the actuator. By controlling the length of the stripe, the bending movement of the actuator can be customized [28]. The relationship between the torque T, the pressure P_m, and the output rotation angle θ can be described as follows [27]:

$$T = -k_r\theta + S_r P_m \tag{4}$$

where k_r is the rotational stiffness of the actuator after constrain, the S_r is the rotational effective area, which can be obtained from the characteristic experiment on the constrained actuator. The constrained SOA could bend up to 90°.

To fully eliminating rigid parts and creating a comfortable wearing experience, the nylon fabric strip is further implemented as the structure of the SSR flipper. The flexible fabrics are easy to fold and bonded into end panels (see Fig. 3).

Two parallel SOAs are mounted on the fabric panels by fixing the end faces using EVA adhesive. The fabric panels work as links that couple the movements of two SOAs. A fabric strip connecting two end panels can be added to obtain flexion. However, the in-plane non-stretchable characteristic of the Nylon fabric hinders the abduction, if the width of the strip is uniform. To achieve two DOF movement, the constrain strip is cut with a kirigami pattern shown in Fig. 4(a). Naturally, a piece

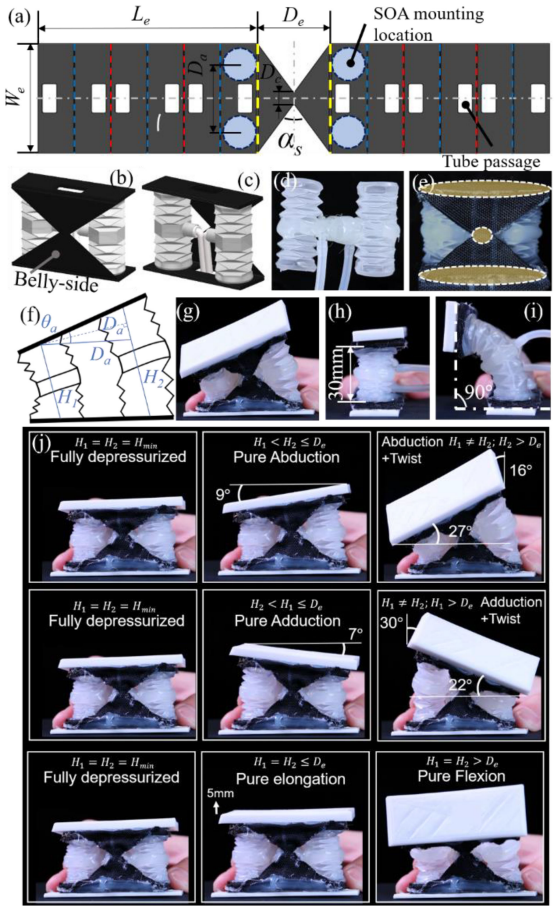

Fig. 4. Design of kirigami patterned Nylon strip and the realization of the joint. (a) Design and parameter of the kirigami strip; (b) belly side and (c) back side of the joint design; the joint was fabricated by (d) first assembling two SOAs with pneumatic fittings, (e) and then attaching the Nylon fabric structure to the SOA assembly, with the glued area marked. The two DOF movements of the SSR joint were displayed: abduction movement is defined in (f) and displayed in (g); flexion movement from (h) fully contract state to (i) 90 degree output. (j) Range of the motions was tested and measured.

of continuous Nylon strip with a kirigami pattern can construct the end panels and the constraint by folding and bonding.

C. Integrated SSR Joint Design

An SSR joint consists of two SOAs and a continuous kirigami fabric strip were proposed. The end panels and the kirigami constrain strip couples the linear movements of two SOAs into two-DOF movements (flexion and abduction).

Two SOAs were parallel placed with end faces glued to two end panels, respectively. Each end panel was made by folding, stocking, bonding six layers of Nylon fabric with EVA adhesive. The red- and blue-dashed lines in Fig. 4(a) indicate the locations of the 180° and −180° folds, respectively. The yellow-dashed lines indicate the locations of 90° folds that connecting the kirigami cut and the end panels. Square windows were cut out from the strip to form the passage for the pneumatic tubes. The kirigami patterned fabric was attached to the SOA at the belly-side of the joint, connecting two end panels [see Fig. 4(b)].

The geometry parameters of the kirigami patterned strip are defined in Fig. 4(a) and listed in Table III. The design of the joint

TABLE III
GEOMETRY OF THE KIRIGAMI FABRICS

L_e	Unfold length of end panel	120mm
W_e	Width of end panel	60mm
D_e	Distance between two end panels	30mm
α_s	Angle of Kirigami cut	73°
D_c	Distance of two cuts	6mm
D_a	Distance of two SOA axes	38mm
T_f	Thickness of Nylon fabric	0.3mm

is shown in Fig. 4(b) and (c). The joint was fabricated as shown in Fig. 4(d) and (e). The glued areas between the fabric and the SOAs are shown in Fig. 4(e). To achieve the desired constraint effect, in the middle of the SSR joint, the fabric is glued to the inlets [see Fig. 4(d)] of the SOAs. The working principle of the SSR joint is similar to a differential mechanism. When two SOAs deform in opposite directions, the joint performs abduction as shown in Fig. 4(g). When two SOAs deforms in the same direction, the joint performs flexion, see Fig. 4(h) and (i). The relationship between the parameters is as follows:

$$W_e = D_c + \frac{D_e}{\tan\frac{\alpha_s}{2}} \tag{5}$$

where the distance between two end panels $D_e = 30$ mm. D_e gives SOA 10 mm to elongate from its fully depressurized length $H_{\min} = 20$ mm without being constrained by the kirigami strip. Therefore, the joint can perform abduction independent of the flexion if the SOA deform within the length range $H \in [H_{\min}, D_e]$. The independent abduction angle θ_a can be obtained as follows:

$$\sin\frac{\theta_a}{2} = \frac{H_2 - H_1}{2D_a} tag6$$

where θ_a is related to the distance between two SOA axes D_a, and the current lengths of actuators H_1 and H_2. According to (6), when the lengths of the actuator $H_1 = H_2$, the abduction angle $\theta_a = 0$, i.e., there is no abduction. Thus, when $H_1 = H_2 > D_e$, the joint performs flexion; when $H_1 = H_2 \leq D_e$, the joint performs linear elongation; when $H_1 \neq H_2$ and $H_1 > D_e$ or $H_2 > D_e$, the joint performs coupled bending.

IV. SSR Flipper Design and Fabrication

A. Proposed SSR Flipper Design

A SSR flipper, consisting of four SSR joints, was proposed as shown in Fig. 5. The geometric parameters are listed in Table III. The joints are consecutively connected by sharing the end panels. Thus, the constrain fabric for the flipper was designed as a continuous strip with kirigami pattern by combining the joint strip design, as shown in Fig. 5(a). The fold lines are indicated by dashed lines similar to the joint. The square windows route pneumatic fittings and tubes inside the flipper. The locations of the windows in each end panel are placed close to the belly-side of the flipper, to minimizing the bending deformation of the tubes, hence the resistance induced by the deformation. A semicircle tip was added to the distal end of the flipper for improving grasp performance.

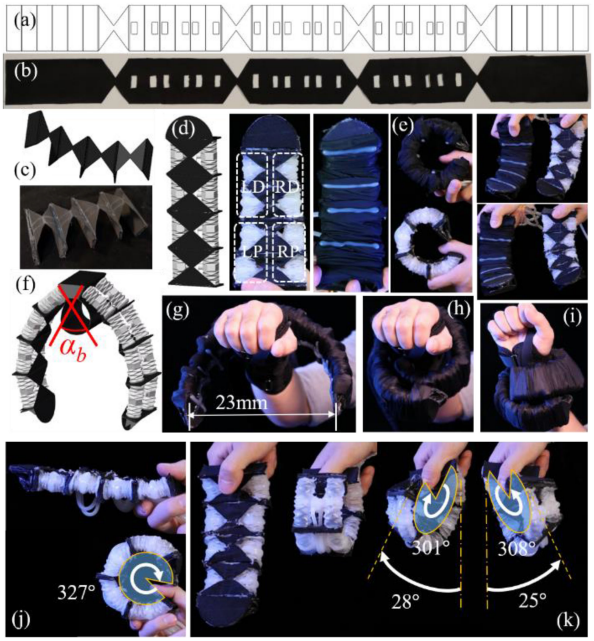

Fig. 5. Design and realization of the SSR flippers. (a) Design of the kirigami strip; (b) prepared Nylon strip; (c) end panels were folded and bonded from the strip; (d) design, fabrication, and wrap of the flipper, each of the LD, RD, LP, RP actuators represent two adjacent synchronized SOAs sharing the same fluid channel; (e) flexion and abduction motions of the flipper with and without the PET fabric wrap, (f) 3D model of the proposed SSR flippers. The angle of the base α_b controls (g) the width of the opening, which in this design reached 23 mm when fully deployed. The grasping movements are demonstrated: (h) the wrap and (i) the hug. The (j) bending and (k) twist ranges of the SSR flipper were tested and measured.

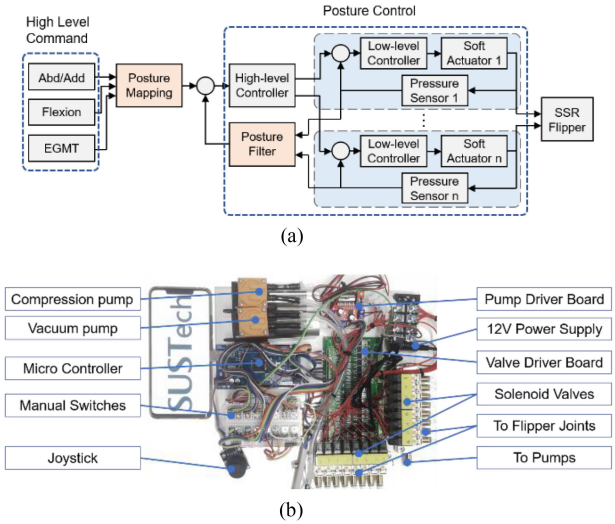

Fig. 6. Actuation and control of the proposed SSR flippers. (a) Control scheme with a cascaded controller structure, while a high-level controller regulates the desired pressure for each actuator, and each actuator controlled by a low-level pressure controller with sensory feedback [34]; (b) actuation system of the proposed flippers, with a compression pump and a vacuum pump driving multiple solenoid valves to supply pressure to the SOAs, controlled by the microcontroller complemented by joystick and switch overrides. The dimensions of the actuation system are 24 cm∗23 cm∗6 cm, the weight is 1.76 kg.

B. Fabrication of the SSR Flippers

First, the fabric strip for one flipper was prepared according to the design as shown in Fig. 5(a)–(d). The length of the kirigami strip is 720 mm, other parameters were the same as the joint. The end panels were folded from the strip following the corresponding lines in the design, and the folded layers were bonded by EVA adhesive. Pneumatic fittings and soft tubes were installed on the actuators. Then, the ends of actuators were glued on the end panels with the tubes routing through the windows. Afterward, the kirigami cut strips were attached. Elastic polyethylene terephthalate (PET) fabrics were wrapped around the flippers to enhance wearing comfort. At the belly of the flipper, soft ridges made of EVA were added at the edges of end panels to increase friction. The fabricated flipper prototype is 205 mm in length and 69 mm in width.

In each flipper, there are eight SOAs arranged in two rows as shown in Fig. 5(d). There are four independent fluid channels. Each channel connects to two adjacent actuators, i.e., the movements are synchronized, each of the LD (Left Distal, SOA 6 and 8), RD (Right Distal, SOA 5 and 7), LP (Left Proximal, SOA 2 and 4), RP (Right Proximal, SOA 1 and 3) actuators represents two adjacent synchronized SOAs sharing the same fluid channel. The LD and RD actuators form an independent joint with two DOF movement; the LP and RP constitute the second independent joint. Thus, a flipper consists of two independent joints and outputs found DOF. The basic motions of the flipper are demonstrated in Fig. 5(e).

Two flippers were assembled on a base that was fixed at the back-hand side of a wristband. In total, the SSR flippers have eight DOF. The tilt angle α_b [see Fig. 5(f)] of the base controls the opening angle of the flippers. In this prototype, angle $\alpha_b = 60^\circ$, the opening width reached up to 230 mm when the flippers fully extended. When worn on the wrist of the user, the base of the flippers located at the back side of the forearm with the flipper handling objects close to the palm.

C. Actuation and Control

The proprietary actuation and control system for the proposed SSR flipper is shown in Fig. 6, which was well documented in [37]. A cascaded control structure was adopted, with a posture-control outer loop and several pressure-control inner loops, each for a soft actuator. The outer loop, controlled by the high-level controller, used pressure feedback information from each actuator to obtain the overall device posture estimation and then compares it with the desired posture mapped from the different control commands (abduction/adduction, flexion, and engagement signal). The resultant pressure commands from the high-level controller were then relayed to the lower-level controllers, each regulating one SOA accordingly.

The actuation system is shown in Fig. 6(b). Two diaphragm pumps (Kamoer KVP8, 12V 9W) supply compressed air and vacuum to the actuators via 16 solenoid miniature pneumatic valves (OST Solenoid SY3/2NC, 12V 1W). Power was supplied via an external battery or 12-V DC adaptors. A microcontroller (Arduino Mega) embeds the control algorithms, with 16 manual switches and a three-way joystick for manual overriding and individual actuator control.

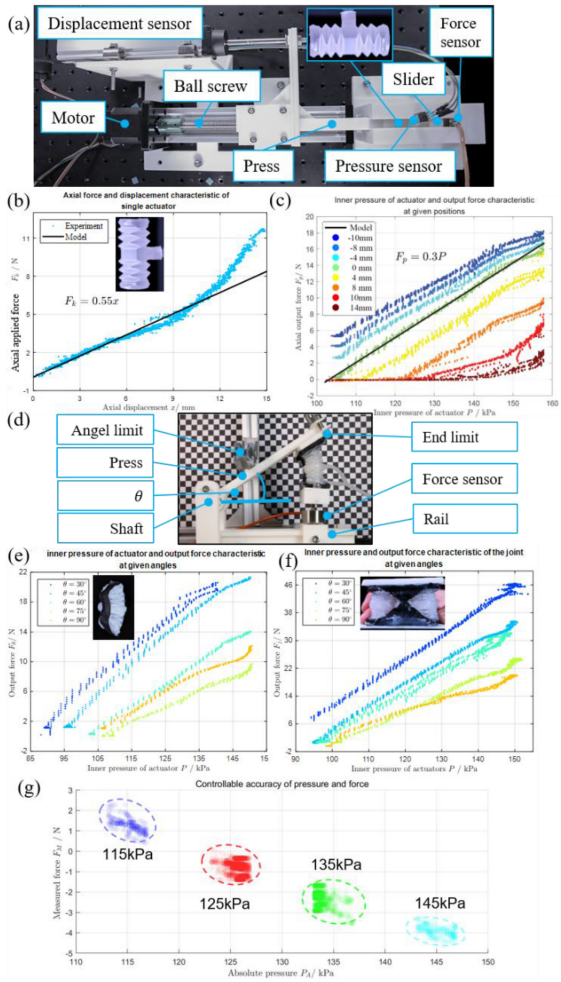

Fig. 7. Tests on the SOA with/without constrain and the SSR joint. (a) Apparatus for testing single SOA, (b) SOA stiffness test results, applied force against resulting axial compression displacement, (c) isometric test result, output force against input air pressure with the SOA fixed at different lengths (for negative displacements, SOA was pre-compressed with contact established with the force sensor; for positive displacements, SOA was not in contact with the force sensor until certain deformation was generated, hence nonlinearity could be observed at lower pressures); (d) test setup for investigating the flexions of the constrained SOA and SSR joint, (e) the inner pressure-output force curves of the constrained SOA were plotted, (f) the inner pressure-output force curves of the SSR joint were plotted. (g) Control performance of the system was tested and plotted.

Each independent joint could be enabled accordingly to perform a combination of maneuvers. For example, the LP (Left Proximal) and RP (Right Proximal) actuators can be enabled to open the flippers without activating the LD (Left Distal) and RD (Left Distal) actuators. In addition, the flexion and abduction movement can be generated by the active joint. Thus, the maneuvers including hugging, grasping, and pinching can be realized.

V. Experimental Validations

A. Actuator Unit Tests

The test setup is shown in Fig. 7(a). A force sensor with a measuring range 0–100 N (DYMH-103, 10 kg, Daysensor) is fixed at the right end of platform. The SOA specimens are placed inside the cylindrical tunnel allowing it to extend and contract. The pneumatic fittings connect the SOA, pump and the air pressure sensor (SSCDANN030PAAA5, 206 kPa, Digi-Key). The friction between the actuator and the tunnel is considered trivial compared to the output force. One end of the actuator is pressing a slider that transmit the force to the force sensor while the other end is limited by the motorized (by a step motor, 6400 steps per revolutions) cylinder press. A displacement sensor (linear potentiometer, Miran 100 mm, 0.5 mm resolution) captures the movement of the cylinder press. In this setup, the air pressure sensor, location of the cylinder press and the output force are recorded.

When the pressure of SOA inner chamber equals the ambient air pressure, linear elastic deformation tests were carried out. The SOA stiffness test results were plotted in Fig. 7(b), where the SOA was passively compressed by external forces. The applied forces were plotted against the resulting axial compression displacement, the curve was fitted by the model in (3), which derived the equivalent coefficient of elasticity $k = 0.55$, hence the force could be calculated. The model fitted closely to the plot curve in the elastic section from 0 to 8 N. After 8 N, the origami folds were completely compressed, the non-linear densification started.

Limiting the linear deformation of the SOA by fixing the positions of the cylinder press, the pressure and force relationship of the SOA isometric test was recorded in Fig. 7(c). The model in (2) were fitted to the curve with 0 mm linear displacement, which derived the effective area of the SOA when pressurized $S = 0.3$. Therefore, the output force of the SOA generated by the inner pressure can be calculated. The curves of different displacements display a parallel distribution, which indicates the slope (effective area of the SOA) is constant. Disparities between curves, especially for positive displacements at lower input pressure levels, were mainly caused by the initial detachment of the SOA and the force sensor. The SOA will only establish contact with the force sensor after sufficient elongation, resulting in the initial nonlinear curve at lower pressures. According to the plot, the SOA (weighing 1.8 g) could achieve axial output forces of 16.5 N, reaching over 900-times its own weight.

The constrained SOA were tested as shown in Fig. 7(d). The test apparatus consists of a revolute press to limit the rotation angle of the constrained actuator, and a force sensor at the fixed end. The angle and end limits were used to fix the position and angle of the free end of the actuator. Relationships of the inner pressure and output force at different angle locations were plotted in Fig. 7(e). The maximum output force 20 N is comparable with the unconstrained SOA (18 N). The constrain strip regulates the movement of SOA without sacrificing the performance.

B. SSR Joint Tests

The test setup is shared with the constraint actuator as shown in Fig. 7(d). Both SOAs of the joint were pressurized simultaneously, performing flexion. The pressure, angular positions, output forces were plotted in Fig. 7(f). The curves displayed linear behavior when the angular positions were limited. The parallel distribution indicates that the effective area for the joint

Fig. 8. Tests on the SSR flippers. (a) Test setup for measuring the maximum payload capacity of the bare-bone prototype at different orientation, (b) the payload plot indicating the SSR flippers were able to carry load as 50 times heavy as its self-weight; (c) when worn on human forearm, the flippers can open, close and compactly wrap around the arm, (d) the flipper were able to perform a combination of abduction/adduction maneuvers in a folded state, displaying the advantages of the dexterity, (e) the adaptiveness to daily objects were demonstrated, a new hugging function was introduced.

is also constant. The maximum output forces are two times of the single constrained SOA, indicating that the output performance of two SOAs was integrated without loss.

The pneumatic control performance of the SSR joint were tested at four different pressure levels, with the force output results plotted in Fig. 7(g). The result shows that the accuracy is limited by the response of the pneumatic control loop, while the repeatability of ± 1 N was achieved.

C. SSR Flippers Tests

Experiments on the grasping performance of the SSR flippers were carried out, including the payload capability, pinching/grasping/hugging motions, and applicability to daily objects. Fig. 8(a) shows the apparatus for measuring the maximum payload capability in different orientation of the flippers. The bare-bone SSR flippers prototype was fixed on the test rig, all the SOAs were fully pressurized at 150 kPa when grasping the payload column, which was connected to the pull handle by non-stretchable threads. In the tests, the flippers overlapped and wrapped around the column. The pull handle was pulled by hand. The force sensor (DYMH-103, 20 kg, Daysensor) at the pull handle recorded the maximum pull forces in corresponding orientations as plotted in Fig. 8(b).

According to the plot, the maximum payload in the vertical direction (0°) is 113 N, i.e., the bare-bone prototype, weighed 225 g, is capable of carrying load as 50 times heavy as its self-weight. This superior payload capacity was achieved by:

1) the non-stretchable Nylon fabrics which can withstand high tensile load in the in-plane directions;
2) the SOAs that formed the overlapping grasp;
3) the friction and the interlocking effect of the end panels at the contacting surface of the two flippers.

The maximum payloads measured at the directions from 15° to 75° are larger than the values from −15° to −75°, respectively. According to the tests, the area where two flippers overlapping were more resistant to the payload than the non-overlapping.

The dexterity of the SSR flippers are demonstrated in Fig. 8(c) and (d). The flippers can compactly wrap around the forearm, see Fig. 8(c), this function enhances the convenience when worn in an unstructured environment. The wide opening of the flippers when fully extended enables the capability to handle objects of a diversity of sizes. The integrated abduction motions of the flippers are displayed in Fig. 8(d). The flippers were able to maneuver in a folded form, this function can be subjected to applications in tight space.

In addition to the dexterity, soft structure and actuation make the flippers adaptive to objects of different shapes. In Fig. 8(e), a variety of daily objects were grasped and picked up by the flippers. Conventional grasping and pinching function were demonstrated, for example, a yellow ball and a water bottle were tightly grasped, a toy dog and a plastic bottle were picked up by pinching. A new "hugging" pattern of object handling was demonstrated, namely, a banana was hugged by the flippers.

VI. Conclusion

In this article, an SSR flipper design was proposed, inspired by the fore flippers of eared seals for their strength, dexterity, as well as flat-shape foldability to maintain streamlining. Differing from the anatomic structure of seal flippers, the proposed SSR flippers used origami soft actuators and kirigami fabric reinforcements to achieve outstanding payload capability during object grasping, while being compliant and foldable with only flexible and soft materials.

A prototype SSR flipper was fabricated and tested to validate the proposed design. For dexterity, the eight-DOF SSR flipper could perform pinching, grasping, and hugging motions, to adapt to different object shapes and sizes, while being able to perform maneuver moves using the two flippers to wrap around the forearm into a compact profile. For payload, the bare-bone SSR flippers weighed merely 225 g without any cover or tubing, while the full set of wearable flippers weighed 460 g with all connection tubing, capable of more than 113 N payload, that is over 24:1 payload to self-weight ratio. The object grasping capabilities and dexterity were demonstrated by a range of experiments using the fabricated prototype, showing excellent object adaptability and versatility.

Future works include developing a portable actuation and control system; developing advanced control algorithms to explore the dexterity of multi-DOF flippers; improving the reinforcement mechanisms to reduce manual fabrication; further investigation on contact layer pattern for improved object grasping stability; carry out human-wearing tests with the flippers to explore the daily usage and interaction with user. This article paves the way to soft wearable robots with balanced strength, dexterity, and compliance, by mass-produced low-cost actuators.

REFERENCES

[1] F. L. Hammond, F. Y. Wu, and H. H. Asada, "Variable stiffness pneumatic structures for wearable supernumerary robotic devices," in *Proc. Adv. Rob.*, 2018, pp. 201–217.

[2] F. Y. Wu and H. H. Asada, "Bio-artificial synergies for grasp posture control of supernumerary robotic fingers," in *Robot., Sci. Systems. X*. Berkeley, USA: University of California, 2014.

[3] F. Y. Wu and H. H. Asada, "Implicit and intuitive grasp posture control for wearable robotic fingers: A data-driven method using partial least squares," *IEEE Trans. Robot.*, vol. 32, no. 1, pp. 176–186, Feb. 2016.

[4] F. Y. Wu and H. H. Asada, "Supernumerary robotic fingers: An alternative upper-limb prosthesis," in *Proc. ASME Dyn. Syst. Control Conf.*, 2014.

[5] T. Ort, F. Y. Wu, N. Hensel, and H. H. Asada, "Supernumerary robotic fingers as a therapeutic device for hemiparetic patients," in *Proc. ASME Dyn. Syst. Control Conf.*, 2015, p. V002T27A010, doi: 10.1115/DSCC2015-9945.

[6] I. Hussain, G. Spagnoletti, G. Salvietti, and D. Prattichizzo, "An EMG interface for the control of motion and compliance of a supernumerary robotic finger," *Front. Neurorobot.*, vol. 10, 2016, Art. no. 18.

[7] H. K. Yap, J. C. H. Goh, and C. H. Yeow, "A low-profile soft robotic sixth-finger for grasp compensation in hand-impaired patients," *J. Med. Devices*, vol. 10, no. 3, Sep. 2016, Art. no. 030914.

[8] F. Parietti, K. C. Chan, B. Hunter, and H. H. Asada, "Design and control of supernumerary robotic limbs for balance augmentation," in *Proc. IEEE Int. Conf. Robot. Automat.*, 2015, pp. 5010–5017.

[9] H. Xie, K. Mitsuhashi, and T. Torii, "Augmenting human with a tail," in *Proc. Aug. Hum. Inter. Conf.*, 2019, pp. 1–7.

[10] A. Kargov, C. Pylatiuk, J. Martin, S. Schulz, and L. Doderlein, "A comparision of the grip force distribution in natural hands and in prosthetic hands," *Disabil Rehabil.*, vol. 26, no. 12, pp. 705–711, 2004.

[11] A. Mohammed *et al.*, "Orochi: Investigating requirements and expectations for multipurpose daily used supernumerary robotic limbs," in *Proc. Aug. Hum. Inter. Conf.*, 2019, pp. 1–9.

[12] I. Hussain, G. Salvietti, G. Spagnoletti, and D. Prattichizzo, "The Soft-sixthfinger: A wearable EMG controlled robotic extra-finger for grasp compensation in chronic stroke patients," *IEEE Robot. Automat. Lett.*, vol. 1, no. 2, pp. 1000–1006, Jul. 2016.

[13] C. James, H. Anita, G. Pierre, S. Ali, and F. Aldo, "The supernumerary robotic 3rd thumb for skilled music tasks," in *Proc. 7th IEEE Int. Conf. Biomed. Robot. Biomechatron.*, Aug. 2018, pp. 665–670.

[14] S. Katz, "Assessing self-maintenance: Activities of daily living, mobility, and instrumental activities of daily living," *J. Amer. Geriatr. Soc.*, vol. 31, no. 12, pp. 721–727, 1983.

[15] A. M. Hart, L. O. Tiziani, J. H. Jung, and F. L. Hammond, "Deformable reflective diaphragm sensors for control of soft pneumatically actuated devices," in *Proc. IEEE Inter. Conf. Soft Robot, RoboSoft*, 2018, pp. 132–139.

[16] S. Liu, F. Wang, Z. Liu, W. Zhang, Y. Tian, and D. Zhang, "A two-finger soft-robotic gripper with enveloping and pinching grasping modes," *IEEE/ASME Trans. Mechatron.*, to be published, doi: 10.1109/TMECH.2020.3005782.

[17] Z. Xie, F. Yuan, Z. Liu, Z. Sun, E. Knubben, and L. Wen, "A proprioceptive soft tentacle gripper based on crosswise stretchable sensors," *IEEE/ASME Trans. Mechatron.*, vol. 25, no. 4, pp. 1841–1850, Aug. 2020.

[18] Y. Li, Y. Chen, Y. Yang, and Y. Li, "Soft robotic grippers based on particle transmission," *IEEE/ASME Trans. Mechatron.*, vol. 24, no. 3, pp. 969–978, Jun. 2019.

[19] C. Friedman and M. Leftwich, "The kinematics of the california sea lion foreflipper during forward swimming," *Bioinspiration Biomimetics*, vol. 9, 2014, Art. no. 046010.

[20] S. J. Godfrey, "Additional observations of subaqueous locomotion in the california sea lion (Zalophus californianus)," *Aquatic Mammals*, vol. 11, pp. 53–57, 1985.

[21] F. E. Fish, "Transitions from drag-based to lift-based propulsion in mammalian swimming," *Amer. Zool.*, vol. 36, pp. 628–641, 1996.

[22] F. E. Fish, "Maneuverability by the sea lion zalophus californianus: Turning performance of an unstable body design," *J. Exp. Biol.*, vol. 206, pp. 667–674, 2003.

[23] K. R. Gordon, "Mechanics of the limbs of the walrus (*Odobenus rosmarus*) and the california sea lion (*Zalophus californianus*)," *J. Morphol.*, vol. 175, no. 1, pp. 73–90. 1983.

[24] Sea Lion Hugs Girl, Aug. 2015. [Online]. Available: https://www.youtube.com/watch?v=fY5RzlD_xDU

[25] Y. Guo, X. Chen, and Z. Wang, "Environmental insulation of 3D printable origanic soft actuators," in *Proc. 9th IEEE Int. Conf. CYBER Technol. Automat., Control, Intell. Syst.*, Aug. 2019, pp. 364–369.

[26] Y. Su *et al.*, "A high-payload proprioceptive hybrid robotic gripper with soft origamic actuators," in *IEEE Robot. Autom. Lett.*, vol. 5, no. 2, 2020, pp. 3003–3010, 2020.

[27] J. Yi *et al.*, "Customizable three-dimensional-printed origami soft robotic joint with effective behavior shaping for safe interactions," *IEEE Trans. Robot.*, vol. 35, no. 1, pp. 114–123, Feb. 2019.

[28] R. V. Martinez, C. R. Fish, X. Chen, and G. M. Whitesides, "Elastomeric origami: Programmable paper-elastomer composites as pneumatic actuators," *Adv. Funct. Mater.*, vol. 22, pp. 1376–1384. 2012.

[29] O. Ivlev, M. Mihajlov, and A. Graser, "Modular multi-sensory fluidic actuator with pleated rotary elastic chambers," *IFAC Proc.*, vol. 39, no. 16, pp. 271–276, 2006.

[30] S. Li, D. M. Vogt, D. Rus, and R. J. Wood, "Fluid-Driven origami-inspired artificial muscles," *Proc. Nat. Acad. Sci.*, vol. 114, no. 50, pp. 13132–13137, 2017.

[31] L. Paez, G. Agarwal, and J. Paik, "Design and analysis of a soft pneumatic actuator with origami shell reinforcement," *Soft Robot.*, vol. 3, no. 3, pp. 109–119, 2016.

[32] I. Hussain, G. Spagnoletti, G. Salvietti, and D. Prattichizzo, "Towards wearable supernumerary robotic fingers to compensate the missing grasping abilities in hemiparetic upper limb," *Int. J. Robot. Res.*, vol. 36, no. 13–14, pp. 1414–1436, 2017.

[33] A. Rafsanjani, Y. Zhang, B. Liu, S. M. Rubinstein, and K. Bertoldi, "Kirigami skins make a simple soft actuator crawl," *Sci. Robot.*, vol. 3, no. 15, 2018, Art. no. eaar7555.

[34] A. Sedal, A. H. Memar, T. Liu, Y. Mengüç, and N. Corson, "Design of deployable soft robots through plastic deformation of kirigami structures," *IEEE Robot. Autom. Lett.*, vol. 5, no. 2, pp. 2272–2279, Apr. 2020.

[35] F. Connolly, D. A. Wagner, C. J. Walsh, and K. Bertoldi, "Sew-free anisotropic textile composites for rapid design and manufacturing of soft wearable robots," *Extreme Mech. Lett.*, vol. 27, pp. 52–58, 2019.

[36] D. Rus and M. T. Tolley, "Design, fabrication and control of origami robots," *Nat. Rev. Mater.*, vol. 3, no. 6, pp. 101–112, 2018.

[37] J. Zhou, X. Chen, U. Chang, Y. Liu, Y. Chen, and Z. Wang, "A grasping component mapping approach for soft robotic end-effector control," in *Proc. 2nd IEEE Int. Conf. Soft Robot, RoboSoft*, 2019, pp. 650–655.

Sicong Liu received the B.S. (Hons.) degree in mechanical design manufacturing and automation and the M.S. degree in mechanical design and theory from the Harbin Institute of Technology (HIT), Harbin, China, in 2009 and 2011, respectively, and the Ph.D. degree in robotics and engineering mechanics from Nanyang Technological University, Singapore, in 2015.

In 2016, he was a Postdoctoral Research Fellow with Nanyang Technological University, Singapore. He was a Mechanical Engineer with the DJI, in 2017. Then, he was a Senior Mechanical Engineer with UBTECH in 2019. He is currently a Research Assistant Professor with the Department of Mechanical and Energy Engineering and the Institute of Robotics, Southern University of Science and Technology, Shenzhen, China. His research interest includes deployable structures inspired by origami and soft robotics.

Yuming Zhu is currently working toward the undergraduate degree in mechanical engineering with the Department of Mechanical and Energy Engineering, Southern University of Science and Technology, Shenzhen, China.

In September 2020, he joined the Department of Mechanical Engineering, Massachusetts Institute of Technology, Cambridge, MA, USA, for a one-year exchange program and will finish his final year project in the SUSTech-MIT Joint Centers for Mechanical Engineering, Education and Research. His research interests include the biomimetic and soft robots.

Zicong Zhang is currently working toward the B.Eng. degree in robotics engineering with the Department of Mechanical and Energy Engineering, Southern University of Science and Technology, Shenzhen, China.

He has worked with the Smart Drone Lab in SUSTech from 2017 to 2019. He is also with the BioRobotics and Control Lab. His research interests include soft robotics and audio analysis.

Zhonggui Fang received the B.S. degree in mechanical design manufacturing and automation from the Guangdong University of Technology, Guangzhou, China, in 2019. He is currently working toward the M.S. degree in mechanics with the Department of Mechanical Engineering and Energy Engineering, Southern University of Science and Technology, Shenzhen, China.

His research interests include soft robotics for medical application and wearable robots.

Jiyong Tan received the B.Eng. degree in electrical information engineering from Zhejiang Algricultural and Forestry University, Hangzhou, China in 2015, and the M.Phil. degree in control engineering from Sichuan University, Chengdu, China, in 2018.

He then served as the Director of Alghorithms in Foxxcon AI Lab and AI engineer at SF Technologies from 2017 to 2018, and as a Technical Director at the AISONO Intelligent Medical Technologies Inc. He is currently a Core Technical Member and Vice Director of the SUSTECH-AISONO Joint Lab in Medical Robotics. His research interests include AI, medical robotics, and soft robotic systems.

Jing Peng received the B.Eng. degree in measurement, control technology and instruments and the Ph.D. degree in mechanical engineering from Tsinghua University, Beijing, China, in 2009 and 2015, respectively.

During her Ph.D. studies, she also carried out research in mechanical and manufacturing engineering at the University of New South Wales as a Professional Practicum student. She was a Postdoctoral Fellow in surgical robotics and soft robotics at the University of Hong Kong. She is currently a Postdoctoral Research Fellow in design robotics for advanced manufacturing with the Queensland University of Technology (QUT). She has several patents granted and she has published articles in materials and processing technologies, soft robotics, and surgical robotics. Her research interests include computer vision, robotics, and pneumatic control.

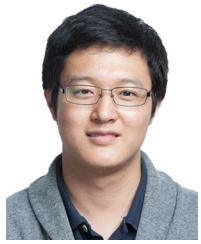

Chaoyang Song received the B.Eng. degree in mechanical engineering from Tongji University, Shanghai, China, in 2009, and the Ph.D. degree in mechanism and robotics from Nanyang Technological University, Singapore, in 2014.

From March 2013 to November 2015, he was a Postdoctoral Research Fellow with the Massachusetts Institute of Technology and the Singapore University of Technology and Design. Then, he was a Lecturer (Assistant Professor) with the Department of Mechanical and Aerospace Engineering, Monash University. He is currently an Assistant Professor with the Department of Mechanical and Energy Engineering and the Institute of Robotics, Southern University of Science and Technology, Shenzhen, China. His research interest includes the design science of bionic robotics and robot learning.

H. Harry Asada (Member, IEEE) received the B.S., M.S., and Ph.D. degrees from Kyoto University, Kyoto, Japan, in 1973, 1975, and 1979, respectively, all in precision engineering.

He is currently the Ford Professor of mechanical engineering and the Director with the Brit and Alex d'Arbeloff Laboratory for Information Systems and Technology, Department of Mechanical Engineering, Massachusetts Institute of Technology, Cambridge, MA, USA. His research in the bio area focuses on bio integrated robots, where live cells and tissues are used as components. He specializes in robotics, biological engineering, and system dynamics and control. His robotics research interests include wearable robots, cellular PZT actuators, and robot applications to aircraft manufacturing and nuclear power plant monitoring.

Dr. Asada was recipient of best paper awards at the IEEE International Conference on Robotics and Automation in 1993, 1997, 1999, and 2010, the O. Hugo Schuck Best Paper Award from the American Control Council in 1985, best journal paper awards from the Society of Instrument and Control Engineers in 1979, 1984, and 1990, and the Best Journal Paper Award from Journal of Advanced Robotics in 2002, Henry Paynter Outstanding Researcher Award from ASME Dynamic Systems and Control in 1998. More recently, he received the 2011 Rufus Oldenburger Medal from ASME and the Ruth and Joel Spira Award for Distinguished Teaching from the School of Engineering, MIT. He is also a Fellow of the American Society of Mechanical Engineers.

Zheng Wang (Senior Member, IEEE) received the B.Sc. degree (Hons.) in automatic control from Tsinghua University, Beijing, China, in 2004, the M.Sc. degree (Hons.) in control systems from the Imperial College London, London. U.K., in 2005, and the Ph.D. degree (Hons.) in electrical engineering from Technische Universitaet Muenchen, Munich, Germany, in 2010.

He was a Postdoctoral Research Fellow with Nanyang Technological University, Singapore, from 2010 to 2013, and a Postdoctoral Fellow with the School of Engineering and Applied Sciences and the Wyss Institute of Bioinspired Engineering, Harvard University, in 2013 and 2014, respectively. Since July 2014, he has been an Assistant Professor with the Department of Mechanical Engineering, The University of Hong Kong, Hong Kong. He has been a Professor of robotics with the Department of Mechanical and Energy Engineering, Southern University of Science and Technology, China, since February 2019. His research interests include haptics human-robot interaction, endoscopic surgical robot, underwater robots, and soft robotics.